RSC Advances

ROYAL SOCIETY OF CHEMISTRY

www.rsc.org/advances

Table of contents

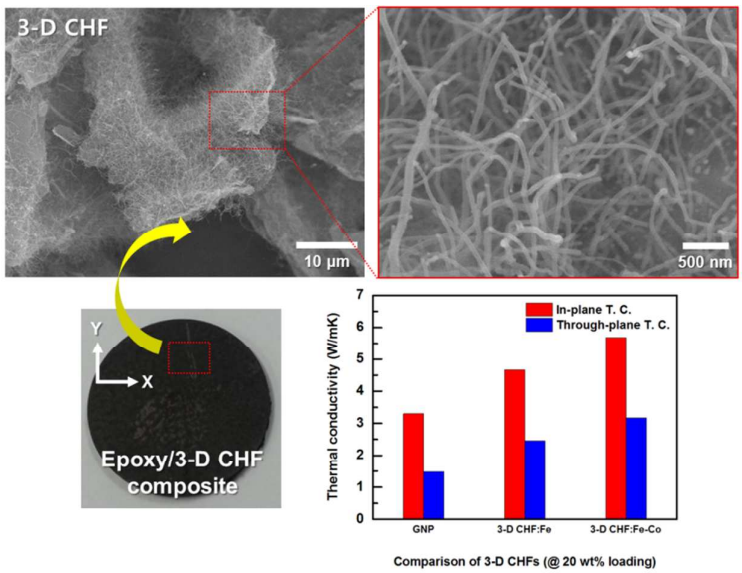

Three-dimensional carbon-based heat dissipating material is newly designed to improve the thermal conductivity of polymer composites at both xy- and z-directions.

Enhanced Thermal Conductivity of Epoxy/Three-Dimensional Carbon Hybrid Filler Composites for Effective Heat Dissipation

Ji Sun Park,*[a] You Jin An,[a] Kwonwoo Shin,[a] Jong Hun Han*[b] and Churl Seung Lee*[a]

[a] Energy Nano Materials Research Center, Korea Electronics Technology Institute (KETI), Seongnam 463-816, Republic of Korea. Fax: +82 31 789 7469; Tel: +82 31 789 7465; E-mail: jisun.park@keti.re.kr (J. S. Park), assong@keti.re.kr (C. S. Lee)

[b] School of Applied Chemical Engineering, Chonnam National University, Gwangju 500-757, Republic of Korea. Fax: +82 62 530 1899; Tel: +82 62 530 1898; E-mail: jhhan@chonnam.ac.kr (J. H. Han)

Abstract

Graphitic carbon nanomaterials (CNMs) are recognized as next-generation heat dissipating materials (HDMs) for efficient thermal conduction within a polymer composite. Commercially used carbon-based HDMs, including carbon blacks, carbon nanotubes (CNTs), and graphites, are limited by low thermal conductivity under 50 % filler content. Two-dimensional graphenes show high thermal conductivity at the direction of the xy-dimension; however, they still exhibit low thermal conductivity at the z-direction because of the hardship of their vertical alignment. Here, we introduce a straightforward strategy to improve the thermal conductivity of graphene-based HDMs at both the xy- and z-directions and investigate on the thermal conductivity behavior of the epoxy composites. Our newly designed graphene-based HDMs present the directly anchored and ohmic-contact morphologies between graphene nanoplatelet (GNP) and CNT via bimetallic nanoparticle decoration on the GNP surface and subsequent CVD process, and their epoxy composites show approximately two-fold enhancement for both in- and through-plane thermal conductivities compared to those of individual GNPs.

1. Introduction

Because of the popularization of high-density electronic devices, thermal management techniques for effective heat dissipation are becoming a critical issue owing to the heat generation that occurs when operating the internal components including batteries, central processing units (CPUs), radio frequency (RF) units, and displays.[1-3] It is known that the heat produced from thermal origin shortens the device's life time by up to 1,500 - 2,000 hours whenever the temperature rises by 1 °C in a device.[4] Thus, electronic devices inevitably require heat dissipating systems such as heat dissipating printed circuit board (PCB), heat spreading sheet, thermal interface material (TIM), and thermal radiation coating between the heat source and the heat sink.[5-8] To date, various heat dissipating materials (HDMs) divided into electrically insulating (SiO_2, SiC, Al_2O_3, BN, AlN, MgO)[9-11] and conducting HDMs (Cu, Al, Ni, Ag, graphite, carbon black, carbon fiber)[12-14] have been generally employed as fillers in a light weight polymer matrix to construct the heat dissipating systems. However, to attain a sufficient thermal conductivity for commercial application (> 5 W/mK), these conventional HDMs have to be filled with high contents (> 50 %) in a polymer matrix, [6, 15, 16] which result in the reduction of mechanical robustness of the polymer composite.

Recently, graphitic carbon nanomaterials (CNMs) including carbon nanotubes (CNTs), graphenes, and multi-layered graphene nanoplatelets (GNPs) have been recognized as next-generation HDMs because of their excellent properties such as light weight, tremendous thermal conductivity (3,000 - 6,000 W/mK), mechanical robustness (Young's modulus ~ 1 Ta), and good dispersibility.[17] In particular, graphenes, which have a large xy-planar dimension, enable numerous area contacts between neighbors in a polymer composite, resulting in the highest thermal conductivity among diverse CNMs.[18-20] However, since two-dimensional graphitic layers are easily re-stacked by the influence of van der Waals force, graphenes tend to horizontally lie down on the substrate, such that anisotropic thermal

conductivity behavior occurs between the directions of the xy-dimension (in-plane) and z-axis (through-plane) regarding the substrate.[21,22] Particularly, vertically-aligned graphenes within the polymer matrix are rarely prepared and difficult to form, development of newly designed CNMs via hybridization is important for enhancing the through-plane thermal conductivity as well as the in-plane thermal conductivity. Indeed, main direction of the heat transfer in the device is one-dimensional heat flow between the heat source and the surroundings.

In previous research, CNTs, carbon fibers, and metal nanowires, which have high thermal conductivities along the z-axis, were incorporated with graphenes to elevate thermal conducting performances by their simple mixing or direct synthesis.[23-28] Among these one-dimensional fillers, CNTs have been considered as an ideal supplementary material because of their high thermal conductivity (3,000 - 6,600 W/mK) comparable to graphenes.[29] However, in the process of their hybridization, a large amount of CNTs leading to much point-type contact geometry[23,26,30] or extra buffer layers on the graphenes prohibiting direct carbon-carbon contacts[30] led to the decrease of thermal conducting performances such that thermal conductivity enhancement at both in- and through-plane directions rarely occurred. In our previous work,[30,31] we investigated GNP-CNT hybrid fillers via CNT synthesis on the GNP surface employing an MgO buffer layer as a metal catalyst support; however, MgO-coated GNPs reduce in-plane thermal conductivity owing to the high interfacial thermal resistance between MgO (45 - 60 W/mK) and GNP, even though through-plane thermal conductivity was enhanced by the vertically-aligned CNTs in an epoxy composite.

Therefore, in this study, we demonstrate a straightforward hybridization strategy of GNP and CNT, without any buffer layers, to improve both in- and through-plane thermal conductivities in an epoxy composite compared with those of individual fillers. Since electroless plating enables simple, controllable, and selective deposition of metals consisting of one more

components regardless of the substrate,[32] GNP surfaces were readily decorated with transition metal nanoparticles via electroless plating. After that, CNTs were successfully hybridized on the GNP surface through the chemical vapor deposition (CVD) process. Epoxy composite with 20 wt% three-dimensional carbon hybrid fillers (3-D CHFs) showed 3.2 times, 2.1 times, and 1.7 times higher through-plane thermal conductivity enhancement and 4.3 times, 1.7 times, and 1.9 times higher in-plane thermal conductivity enhancement than those of individual CNT, GNP, and simply mixed GNP/CNT fillers, respectively.

2. Experimental

Materials

GNP and CNT were purchased from XG Science (grade: M-25, USA) and Nanocyl (grade: NC 7000, USA), respectively. Tin chloride ($SnCl_2$), palladium chloride ($PdCl_2$), sodium hypophosphite monohydrate ($NaPO_2H_2 \cdot H_2O$), citric acid, boric acid, sodium hydroxide (NaOH), iron sulfate heptahydrate ($FeSO_4 \cdot 7H_2O$), cobalt sulfate heptahydrate ($CoSO_4 \cdot 7H_2O$), and hydrochloric acid (HCl, 37 %) were purchased from Sigma-Aldrich (USA). Bisphenol A-type epoxy resin (Kukdo Chemical: KFR-120) and amine-based epoxy hardener (Kukdo Chemical: KFH-150) were kindly provided by Kukdo Chemical (Republic of Korea).

Preparation of 3-D CHFs

The procedure to decorate metal nanoparticles on the GNP surface is composed of three steps: (1) sensitization, (2) activation, and (3) electroless plating. Firstly, GNPs were sensitized in an acidic $SnCl_2$ solution (H_2O:HCl = 125:1, v/v) using a bath-type sonicator for 60 minutes, and were then washed with deionized water using micro-mesh-sized sieves to remove the non-reacted residuals. These sensitized GNPs were activated in an acidic $PdCl_2$ solution (H_2O:HCl = 400:1, v/v) for 60 minutes in a bath-type sonicator, and then similarly washed as mentioned above. The pre-treated GNPs were decorated with Fe monometallic nanoparticles or Fe-Co

bimetallic nanoparticles by an electroless plating, which was performed in an alkaline solution containing NaOH, $FeSO_4 \cdot 7H_2O$ (metal precursor 1), $CoSO_4 \cdot 7H_2O$ (metal precursor 2), $NaPO_2H_2 \cdot H_2O$ (reducing agent), citric acid (complexing agent), and boric acid (buffering agent) for at 90 °C. For removing the residuals, Fe or Fe-Co decorated GNPs were cleaned with deionized water using micro-mesh-sized sieves.

For directly hybridizing the CNTs on the GNP surface, Fe or Fe-Co decorated GNP powders were placed in an open sintered pure alumina boat and thermally treated under an Ar (500 sccm) gas flow in a horizontal quartz tube furnace (70 mm diameter, 1400 mm length) for 20 minutes at 800 °C. H_2/C_2H_2 (40 sccm / 60 sccm) mixed gas flow was applied for 20 minutes at the same temperature and then cooled down to room temperature under an Ar (500 sccm) gas flow.

Fabrication of epoxy/3-D CHFs composite

The epoxy composites containing 3-D CHFs were fabricated according to the following steps. Firstly, 20 wt% 3-D CHFs were added to the bisphenol A-type epoxy resin (Kukdo Chemical: KFR-120) and homogeneously mixed with a shear mixer (THINKY Super Mixer: SR-500) for 5 minutes at a speed of 1200 rpm. Amine-based epoxy hardener (Kukdo Chemical: KFH-150) was subsequently added to the epoxy/3-D CHFs suspension and shear mixing was performed for 5 minutes at the same rpm speed. The prepared epoxy/3-D CHFs mixture was molded by hot-press equipment (QMESYS heating press tester: QM900M) and cured for 50 minutes at 80 °C. At the gel point, post-curing was additionally performed for 70 minutes at the same temperature. The size of prepared circular epoxy composites was 12.7 mm (through-plane sample) or 25.4 mm (in-plane sample) in diameter and 1.0 mm in thickness. Since thickness variation of the composite may interrupt the reliability of its thermal conductivity, thickness of all samples were identically fabricated without further polishing process. Besides,

in order to avoid the formation of pores within the epoxy composite including its surface, which greatly affects the thermal conductivity, all samples were carefully prepared.

Characterization

Surface morphologies of the 3-D CHFs were characterized by field-emission scanning electron microscope (FE-SEM, Hitachi S-4800, accelerating voltage: 15 kV), and transmission electron microscope (TEM, JEM-2100F, JEOL). Surface ingredients of the metal deposited GNPs were analyzed by energy-dispersive X-ray spectroscopy (EDX, GENESIS 2000, EDAX). The contents of Fe, Sn, and Pd within the 3-D CHFs were investigated by a thermogravimetric measurement (TGA 2950, TA instrument) system. To identify the crystallinity of the CNTs, Raman spectroscopy measurement (514.5 nm laser, LabRam HR, Horiba Jobin–Yvon) was performed. Thermal conductivity of the epoxy composite was measured by the laser flash method (LFA 447 Nanoflash, Netzsch), which has generally been a standard and popular technique for measuring thermal diffusivities of solid materials above room temperature. We note that additional graphite spray-coating was employed on the surface of composite sample to enhance the absorption of Xenon light pulse energy and emission of infrared (IR) radiation at the sample's front and back surface. However, measured thermal diffusivities were not different regardless of whether graphite spray-coating was performed or not in case of our epoxy/3D-CHFs composites at 20 - 50 wt% filler-loading.

3. Results and Discussion

Fig. 1(a) shows the experimental procedure for preparing the 3-D CHFs. To directly grow the CNTs on the GNP surface, pristine GNP powders were pre-treated with Pd/Sn components and readily decorated with Fe nanoparticles via electroless plating. After the process of metal-catalyst-loading on the GNP surface, CNTs were spontaneously synthesized on a GNP surface such as downy hairs in all directions through the CVD process. Fig. 1(b) presents the SEM

image of the Fe decorated GNP surface before CNT synthesis, and its surface ingredients were analyzed using EDX measurement in Fig. 1(c). From the result of EDX, we identified that GNP surfaces were successfully decorated with Fe nanoparticles via electroless plating. The 3-D CHFs with directly anchored junctions between GNP and CNT were finally prepared in Fig. 1(d). To investigate more detailed junction points between them, we additionally took a TEM image (Fig. 1(e)) and found the direct anchoring points in an inset of Fig. 1(e). Since the Fe catalyst was situated at the top of the CNT, GNP and CNT formed a direct ohmic contact without interlayers; this tip-growth mechanism of the CNT synthesis is mainly attributed to the weak physical adhesion between GNP surface and Fe catalyst. In more detail, during the CVD process, hydrocarbons decomposed on the top surface of Fe catalyst, and carbons diffused down through the metal. Then, CNT precipitated out across the metal bottom, pushing the whole metal catalyst off the GNP surface.[33] From now on, 3-D CHFs prepared from Fe monometallic nanoparticles will express as a "3-D CHF:Fe".

Figs. 2(a)-(c) show the surface morphologies of 3-D CHF:Fe with 15 %, 30 %, and 55 % CNT content. We note that the CNT content on the GNP surface was calculated from the mass difference between before and after CNT growth (equation (1)).

$$\text{CNT Content (\%)} = \frac{m_1 - m_0}{m_0} \times 100, \qquad (1)$$

where m_0 is the mass of Fe decorated GNP before CNT growth, and m_1 is the mass of 3D-CHF:Fe after CNT growth. The CNT content on the GNP surface was readily controlled by altering the amount of metal precursor ($FeSO_4 \cdot 7H_2O$) at the stage of electroless plating. As the amount of metal precursor increased, more CNTs were synthesized on the GNP surface during the CVD process. Furthermore, CNT population on the individual GNP surface and average CNT diameter (20 nm → 50 nm) had also proportionately risen.

To investigate the presence of defects on the CNTs within a 3-D CHF:Fe, Raman spectroscopic measurement was performed in Fig. 3(a). For sample preparation, we selectively gathered CNTs via sonication, centrifugation, and extraction of 3-D CHF:Fe/N-methyl-2-pyrrolidone (NMP) dispersion, and gathered CNT solution was subsequently spray-coated on a slide glass. As shown in a graph, CNTs presented D, G, and 2D bands at 1,341 cm^{-1}, 1,596 cm^{-1}, and 2,716 cm^{-1}, respectively, and calculated I_G/I_D ratio was 0.88. This indicates that CNTs were successfully grown on the GNP surface without severe distortion of their graphitic structures. Furthermore, to confirm the amount of metal catalysts or impurities (Fe, Sn, Pd) within a 3-D CHF:Fe, we analyzed the samples via TGA measurement in Fig. 3(b). The result was that GNP and 3-D CHF:Fe with 15 %, 30 %, and 55 % CNT content included 0.8 %, 3.2 %, 5.2 %, and 6.6 % inorganic metal catalysts or impurities, respectively, and these values were increased proportionately with the quantity of initial metal precursors.

With designed 3-D CHFs:Fe, we investigated thermal conductivity characteristics of epoxy/3-D CHF:Fe composites in Fig. 4. The epoxy composite was prepared by dispersing the 3-D CHFs:Fe in bisphenol A-type epoxy resin/amine-based epoxy hardener suspension and by molding the 3-D CHFs:Fe/epoxy/hardener suspension using hot press equipment. Fig. 4(a) shows the relationship of thermal conductivity (in- & through-plane) versus CNT content within a 3-D CHF:Fe at 20 wt% total filler-loading in an epoxy matrix. In the case of through-plane thermal conductivity, CNTs ranging from 15 % to 55 % content on the GNP surface effectively raised the vertical thermal conductance of the epoxy composite compared with the reference (GNP/epoxy composite, CNT content: 0 %) and maximized at the 15 % CNT content. However, in case of in-plane thermal conductivity, there was the optimum CNT content of 15 % on the GNP surface, and large amount of CNTs on the GNP surface hindered horizontal thermal conductance of the epoxy composite in comparison with the reference. It is believed that numerous CNTs on the GNP surface led to a great deal of point-type contact

geometry at the neighboring GNP interfaces, resulting in the disturbance of direct area contact between GNPs,[23] and the incomplete wetting of epoxy resins between CNTs within a 3-D CHF:Fe, resulting in the formation of interstitial air.[34] Thus, we determined that the optimum CNT content within a 3-D CHF:Fe is approximately 15 % to enhance both in- and through-plane thermal conductivities. In Fig. 4(b), thermal conductivities of epoxy composites with various carbon fillers including CNT, GNP, simply mixed GNP/CNT, and 3-D CHF:Fe were directly compared to confirm the degree of enhancement of our 3-D CHF:Fe at 20 wt% total filler-loading. To characterize the thermal conductivity of simply mixed GNP/CNT fillers in the epoxy composite, we used NC 7000 grade CNTs (Nanocyl) with 15 % of GNP mass. As CNTs were incorporated with the GNPs whether they were simply mixed or directly hybridized, through-plane thermal conductivities of epoxy composites were effectively enhanced up to 1.7 times compared to that of the GNP fillers. However, unlike directly hybridized 3-D CHFs:Fe, the in-plane thermal conductivity of the simply mixed GNP/CNT fillers showed a decreased value compared to that of the GNP fillers. This performance reduction is attributed to the non-homogenous dispersion of individual GNP and CNT fillers in an epoxy matrix originated from the density difference between them (GNP (2.2 g/cm^3), CNT (1.7 g/cm^3)). Consequently, effective thermal conducting pathways were not formed by the CNTs between horizontally-laid GNPs in an epoxy matrix. To investigate the effect of total filler content in an epoxy composite for higher thermal conductivity, 20 - 35 wt% 3-D CHFs:Fe (CNT content: 15 %) were loaded in an epoxy matrix, and their thermal conductivities were characterized in Figs. 4(c) and 4(d). Within the ranges, 3-D CHFs:Fe (CNT content: 15 %) effectively enhanced both in- and through-plane thermal conductivities compared to those of GNP fillers. In more detail, 3-D CHFs exhibited 1.4 times (@ 20 wt%), 1.1 times (@ 25 wt%), 1.2 times (@ 30 wt%), and 1.1 times (@ 35 wt%) higher in-plane thermal conductivity enhancement, and 1.7 times (@ 20 wt%), 1.5 times (@ 25 wt%), 1.3 times (@ 30 wt%), and 1.1 times (@ 35 wt%) higher through-plane thermal conductivity

enhancement, respectively, compared to the GNP fillers at the same filler loading. Because of the increase of 3-D CHF:Fe content (20 wt% → 35 wt%) in an epoxy composite, their thermal conductivity enhancements were gradually saturated compared with the reference. And, 3-D CHFs:Fe have more effectively influenced on the thermal conductivity enhancement of epoxy composite at the smaller filler content.

To directly confirm the distribution of 3-D CHFs:Fe within the epoxy composite, the samples were slightly calcined at 400 °C for 5 minutes and observed using SEM equipment. The inset of the Fig. 5(a) shows the raw sample of the epoxy composite before calcination, and Figs. 5(a) and 5(b) present the calcined plane- and cross-sectional-view of the sample, respectively. As shown in the figure, CNTs effectively bridged between neighboring GNPs in all directions, resulting in higher both in- and through-plane thermal conductivities than those of epoxy/GNP composite at the same filler-loading. It implies that CNTs effectively bridged between neighboring GNPs without breaking the GNP's main orientation and crystallinity and provided additional heat flowing pathways without severe thermal resistance at the GNP/CNT/GNP interfaces.

Furthermore, for improving the quality of CNTs on the GNP surface, bimetallic nanoparticles composed of two ingredients (Fe and Co) were employed on the GNP surface as a catalyst instead of the monometallic Fe nanoparticles, taking advantage of the electroless-plating deposition. The detailed experimental procedure was shown in Fig. 6(a), and $CoSO_4 \cdot 7H_2O$ (metal precursor 2) was additionally inserted at the stage of electroless plating in Fig. 1(a). The morphology of 3-D CHFs synthesized from Fe-Co alloy nanoparticles (3-D CHFs:Fe-Co) on the GNP surface was presented in Figs. 6(b) and 6(c). Unlike the morphology of Fig. 2, CNTs on the GNP surface exhibited straighter morphology than that of the CNTs synthesized from monometallic Fe nanoparticles. This morphological difference is attributed to the

stability of Fe-Co ($Fe_{0.85}C_{0.15}$) bimetallic catalysts towards oxidation and carburization reaction avoiding the formation of Fe_3C, such that bimetallic catalyst was beneficial for the formation of multi-walled CNTs.[35] Figs. 6(d) and 6(e) present the TEM images of synthesized multi-walled CNTs on the GNP surface. With optimized 3-D CHFs:Fe-Co, the thermal conductivities of epoxy composites with 20 wt% total filler loading were characterized in Fig. 6(f) and directly compared with those of 3-D CHFs:Fe and GNP fillers. According to the morphology alteration of CNTs from twisty (Fig. 2(d)) into straight shapes (Fig. 6(c)) within a 3-D CHF, in- and through-plane thermal conductivities showed 1.2 times and 1.7 times higher in-plane thermal conductivity enhancement and 1.3 times and 2.1 times higher through-plane thermal conductivity enhancement compared with the 3-D CHF:Fe (in-plane: 4.7 W/mK, through-plane: 2.5 W/mK) and GNP fillers (in-plane: 3.3 W/mK, through-plane: 1.5 W/mK), respectively.

The surface morphology of calcined epoxy composite with 3-D CHFs:Fe-Co was shown in Figs. 7(a) (plane view) and 7(b) (cross-sectional view). The CNTs with straight shapes were more effectively linked with neighboring GNPs than those of 3-D CHFs:Fe (Fig. 5). From Raman spectroscopic measurement (Fig. 7(c)), I_G/I_D ratio was confirmed with 1.06, which value corresponds to a 1.2 times improvement compared to that of 3-D CHFs:Fe (I_G/I_D = 0.88). In Fig. 7(d), we characterized thermal conductivity behavior of epoxy/3-D CHF composites with high total filler content of 46.5 wt% to confirm the maximized thermal conductivity of the composite under 50 wt% filler content. Our 3-D CHFs:Fe-Co presented an in-plane thermal conductivity of 30.96 W/mK and through-plane thermal conductivity of 4.32 W/mK in an epoxy composite. These values correspond to an improvement of 1.5 times (in-plane) and 1.2 times (through-plane), respectively, compared with the GNP fillers.

4. Conclusion

We have demonstrated 3-D CHF preparation and its application into heat dissipating epoxy composites. Since electroless-plating deposition enables the simple formation of multi-component metal nanoparticles on an arbitrary substrate, catalytic metal nanoparticles (Fe or Fe-Co), which are beneficial for direct CNT growth, were successfully decorated on the non-reactive pristine GNP surfaces. From catalytic metal nanoparticles, 3-D CHFs were readily synthesized via the CVD process, and their surface morphologies exhibited directly anchored and ohmic-contact structure between GNP and CNT. The 3-D CHF in an epoxy matrix showed efficient heat conduction at both in- and through-plane directions via additional heat conducting pathways that were formed by CNTs (nano-sized filler) bridged between neighboring GNPs (micro-sized filler). This work manifests that properly designed three-dimensional carbon-structured fillers via a directly anchored hybridization process may provide a better thermal conducting property within the thermoplastic/thermosetting polymer composites compared with the single carbon filler. Furthermore, our approach offers a convenient, effective, and mass-producible method to hybridize different kinds of carbon nanomaterials and opens up diverse potential applications, ranging from heat dissipating materials to electrode materials.

Acknowledgements

This study was supported by World Premier Materials (WPM) Program (10037890), and the Industrial Strategic Technology Development Program (10041851) funded by the Ministry of Trade, Industry & Energy (MI) of Korea.

References

1 S. P. Gurrum, S. K. Suman, Y. K. Joshi, and A. G. Fedorov, *IEEE T. Device Mat. Re.,* 2004, **4**, 709.

2 J. Wei, *Heat Transfer Eng.* 2008, **29**, 178.

3 V. Singhal, T. Siegmund, and S. V. Garimella, *IEEE T. Comp. Pack. Man.,* 2004, **27**, 244.

4 S. Keeping, LED Heat Dissipation and Lowering Thermal Resistance of LED Lighting Substrates, http://www.digikey.com/en/articles/techzone/2011/aug/led-heat-dissipation-and-lowering-thermal-resistance-of-led-lighting-substrates, accessed: 2, 2011.

5 S. Cho, and J. Y. Lee, *Electron. Mater. Lett.,* 2010, **6**, 167.

6 R. Prasher, *P. IEEE,* 2006, **94**, 1571.

7 R. Siegel, and J. Howel, *Thermal Radiation Heat Transfer 4th edition*, Tayler & Francis, New York, NY, USA 2002.

8 Y. -A. Sha, Y. -S. Jhuo, K. –H. Chen, and S. -C. Wang, in *Microsystems, Packaging, Assembly and Circuits Technology Conference (IMPACT) 2013 8th international* (*IEEE 2150-5934)*, IEEE, Piscataway, NJ, USA 2013, 74.

9 Y. Hwang, M. Kim, and J. Kim, *RSC Adv.,* 2014, **4**, 17015.

10 T. -L. Li, and S. L. -C. Hsu, *J. Phys. Chem. B,* 2010, **114**, 6825.

11 E. -S. Lee, and S. -M. Lee, *J. Am. Ceram. Soc.,* 2008, **91**, 1169.

12 S. Wang, Y. Cheng, R. Wang, J. Sun, and L. Gao, *ACS Appl. Mater. Interfaces,* 2014, **6**, 6481.

13 C. Lin, and D. D. L. Chung, *Carbon,* 2009, **47**, 295.

14 E. Bekyarova, E. T. Thostenson, A. Yu, H. Kim, J. Gao, J. Tang, H. T. Hahn, T.-W. Chou, M. E. Itkis, and R. C. Haddon, *Langmuir,* 2007, **23**, 3970.

15 F. Sarvar, D. C. Whalley, and P. P. Conway, in *Electronics System Integration Technology Conference (IEEE 1-4244-0553)*, Vol. 2, IEEE, Piscataway, NJ, USA 2006, 1292.

16 R. S. Prasher, J. -Y. Chang, I. Sauciuc, S. Narasimhan, D. Chau, G. Chrysler, A. Myers, S. Prstic, and C. Hu, *Intel Technol. J.,* 2005, **9**, 285.

17 S. H. Lee, D. H. Lee, W. J. Lee, and S. O. Kim, *Adv. Funct. Mater.,* 2011, **21**, 1338.

18 A. A. Balandin, S. Ghosh, W. Bao, I. Calizo, D. Teweldebrhan, F. Miao, and C. N. Lau, *Nano Lett.*, 2008, **8**, 902.

19 S. H. Song, K. H. Park, B. H. Kim, Y. W. Choi, G. H. Jun, D. J. Lee, B. -S. Kong, K. -W. Paik, and S. Jeon, *Adv. Mater.*, 2013, **25**, 732.

20 K. M. F. Shahil, and A. A. Balandin, *Nano Lett.*, 2012, **12**, 861.

21 A. A. Balandin, *Nat. Mater.*, 2011, **10**, 569.

22 E. Pop, V. Varshney, and A. K. Roy, *MRS bulletin*, 2012, **37**, 1273.

23 A. Yu, P. Ramesh, X. Sun, E. Bekyarova, M. E. Itkis, and R. C Haddon, *Adv. Mater.*, 2008, **20**, 4740.

24 Q. -Q. Kong, Z. Liu , J. -G. Gao, C. -M. Chen, Q. Zhang, G. Zhou, Z. -C. Tao, X. -H. Zhang, M. -Z. Wang, F. Li, and R. Cai, *Adv. Funct. Mater.*, 2014, **24**, 4222.

25 V. H. Luan, H. N. Tien, T. V. Cuong, B. -S. Kong, J. S. Chung, E. J. Kim, and S. H. Hur, *J. Mater. Chem.*, 2012, **22**, 8649.

26 W. Feng, J. Li, Y. Feng, and M. Qin, *RSC Adv.*, 2014, **4**, 10090.

27 A. Dichiara, J. -K. Yuan, S. -H. Yao, A. Sylvestre, and J. Bai, *J. Nanosci. Nanotechnol.*, 2012, **12**, 6935.

28 W. Li, A. Dichiara, and J. Bai, Compos. Sci. Technol., 2013, **74**, 221.

29 S. Berber, Y. -K. Kwon, and D. Tománek, *Phys. Rev. Lett.,* 2000, **84**, 4613.

30 L. Yu, J. S. Park, Y. -S. Lim, C. S. Lee, K. Shin, H. J. Moon, C. -M. Yang, Y. S. Lee, and J. H. Han, *Nanotechnology*, 2013, **24**, 155604.

31 L. Yu, H. Kang, Y. S. Lim, C. S. Lee, K. Shin, J. S. Park, and J. H. Han, *J. Nanosci. and Nanotechnol.,* 2014, **14**, 9139.

32 M. Schlesinger, and M. Paunovic, Modern Electroplating 5th edition, Wiley, Hoboken, NJ, USA 2010.

33 M. Kumar, and Y. Ando, *J. Nanosci. Nanotechnol.*, 2010, **10**, 3739.

34 A. M. Marconnet, N. Yamamoto, M. A. Panzer, B. L. Wardle, and K. E. Goodson, *ACS Nano*, 2011, **5**, 4818.

35 P. Coquay, A. Peigney, E. D. Grave, E. Flahaut, R. E. Vandenberghe, and C. Laurent, *J. Phys. Chem. B,* 2005, **109**, 17813.

Figures & Captions

Fig. 1. (a) Experimental procedure for preparing the 3-D CHF:Fe. (b) SEM image of Fe decorated GNP surface prepared by electroless-plating deposition, and (c) its EDX surface analysis. Surface morphologies of synthesized 3-D CHF:Fe investigated by (d) SEM and (e) TEM measurements.

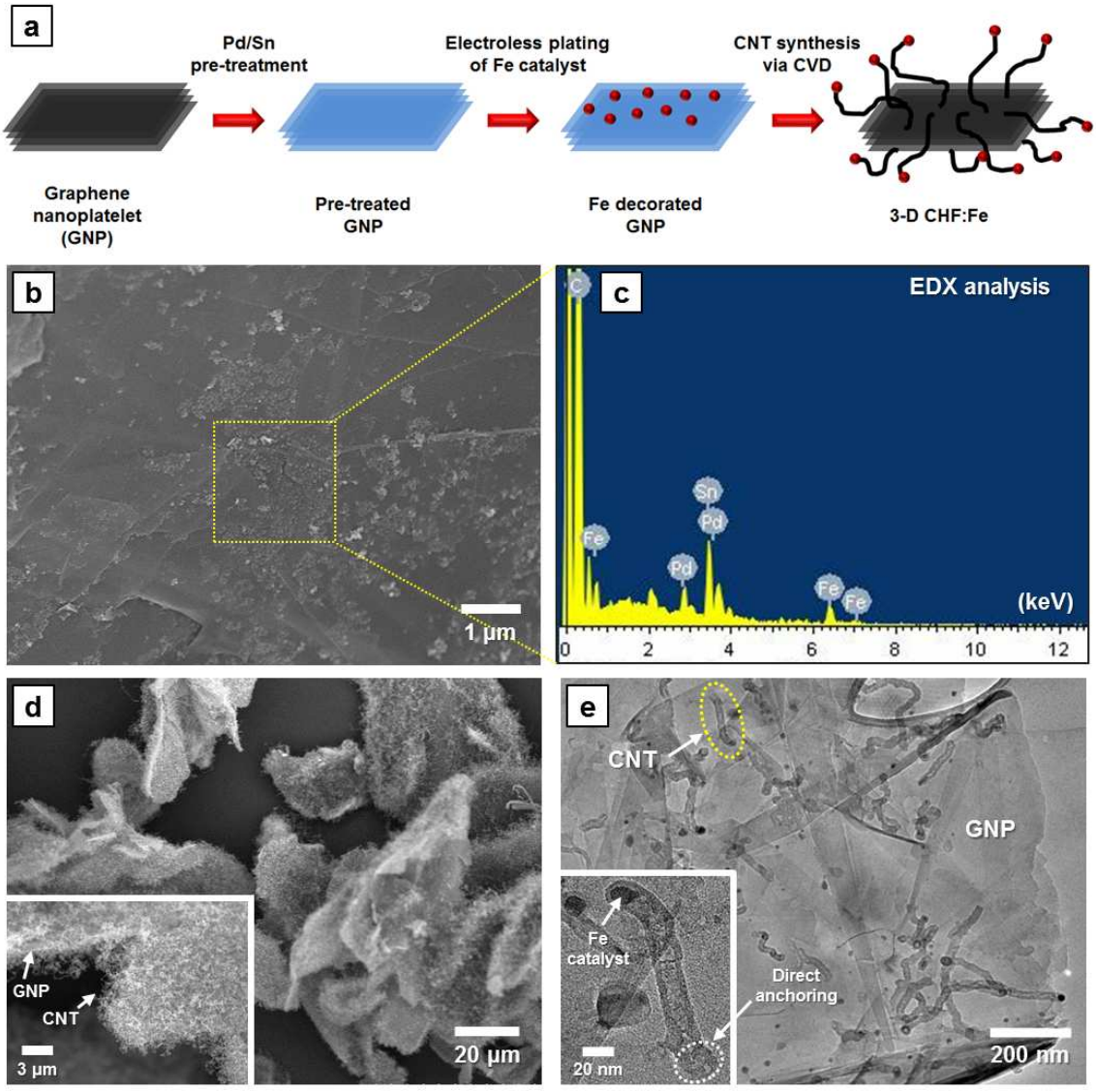

Fig. 2. The 3-D CHF:Fe with (a, d) 15 %, (b, e) 30 %, and (c, f) 55 % CNT content. (d), (e), (f) Magnified images of 3-D CHF:Fe surface.

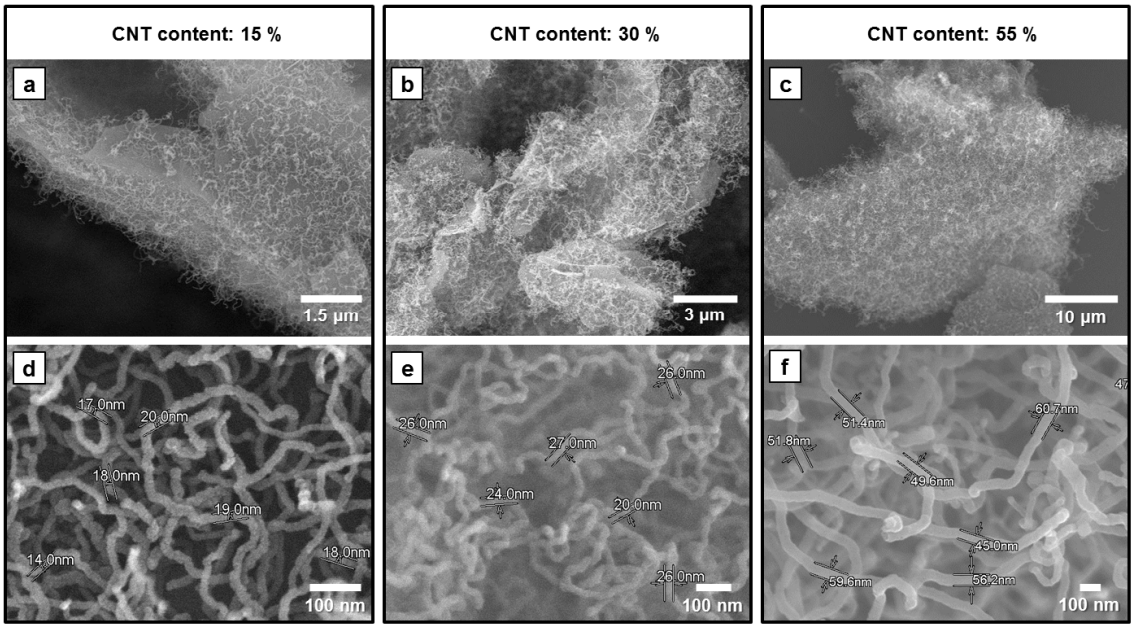

Fig. 3. (a) Raman spectra of CNTs within a 3-D CHF:Fe. (b) TGA analysis of 3-D CHF:Fe with various CNT content (15 %, 30 %, 55 %).

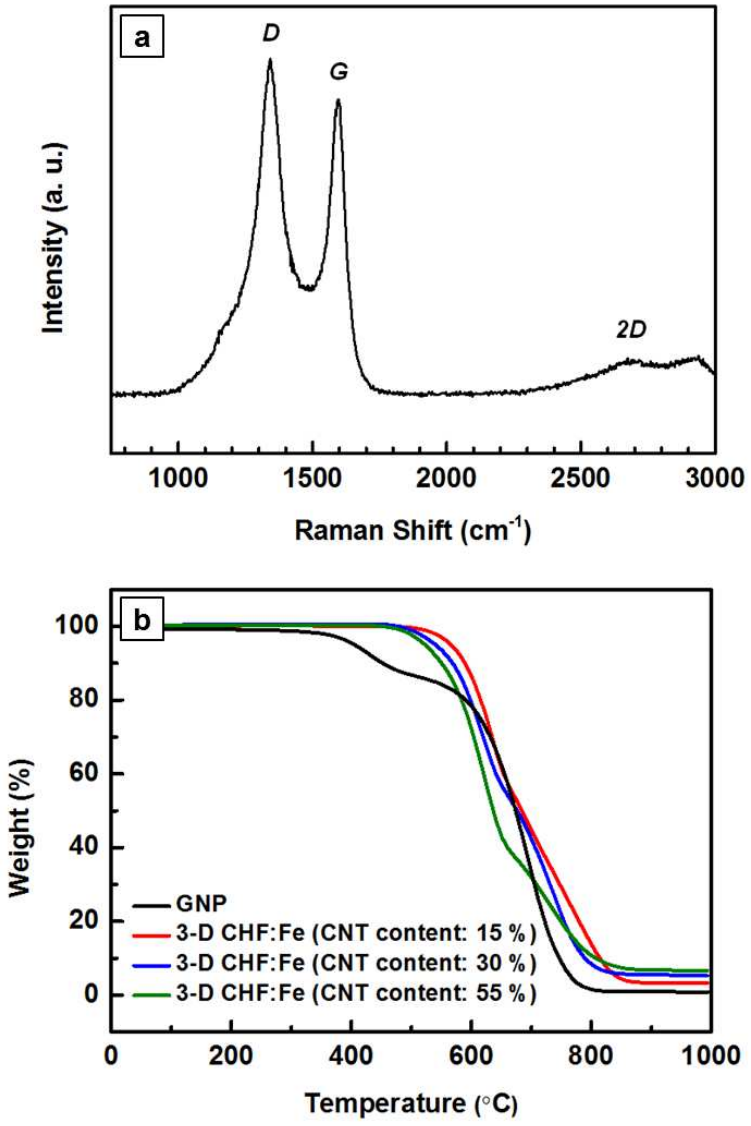

Fig. 4. (a) Thermal conductivity of epoxy/3-D CHF:Fe composites with various CNT content (15 %, 30 %, 55 %) within a 3-D CHF:Fe at 20 wt% total filler-loading. (b) Comparison of thermal conductivities of epoxy composites with various carbon fillers (CNT, GNP, simply mixed GNP/CNT, and 3-D CHF:Fe) at 20 wt% total filler-loading. (c) In- and (d) through-plane thermal conductivities of epoxy/3-D CHF:Fe composites with 15 % CNT content at various total filler-loading (20 wt%, 25 wt%, 30 wt%, 35 wt%).

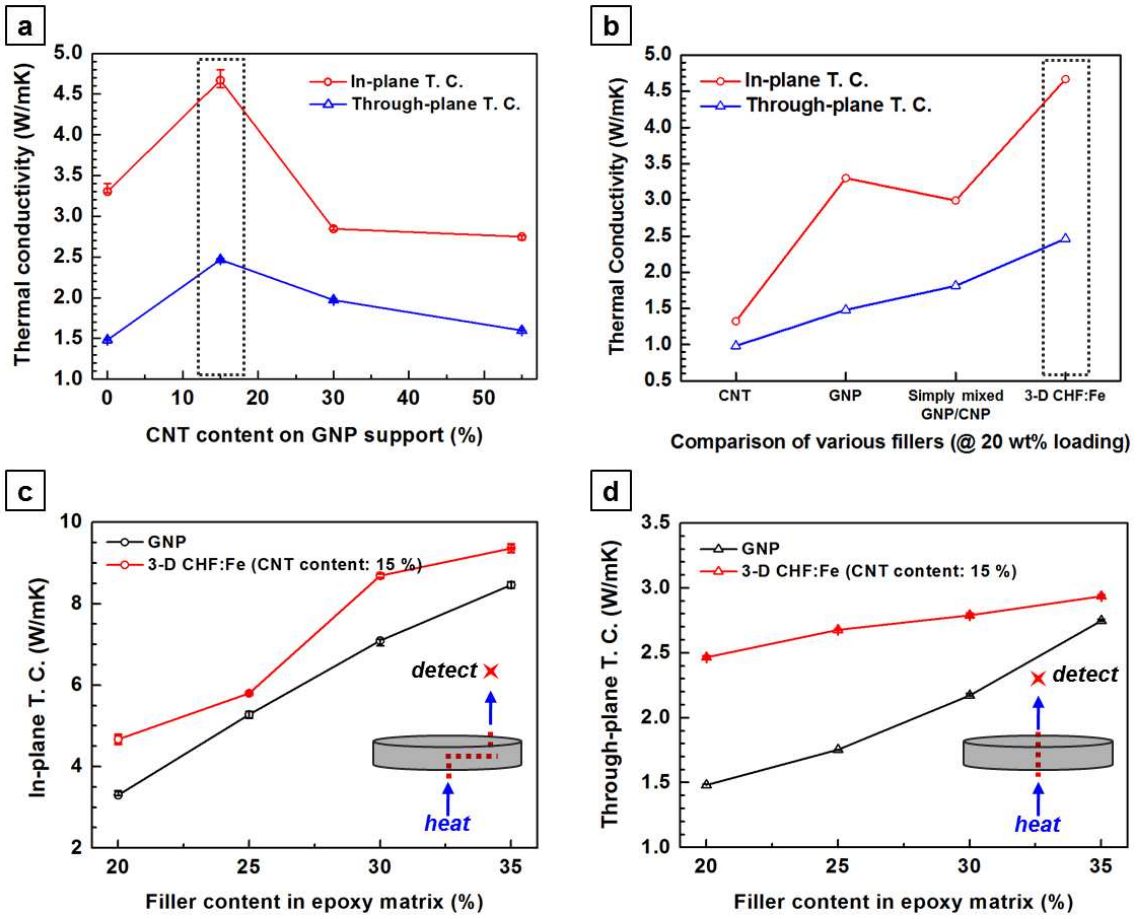

Fig. 5. SEM images of calcined epoxy/3-D CHF:Fe composites. (a) Plane- and (b) cross-sectional-view.

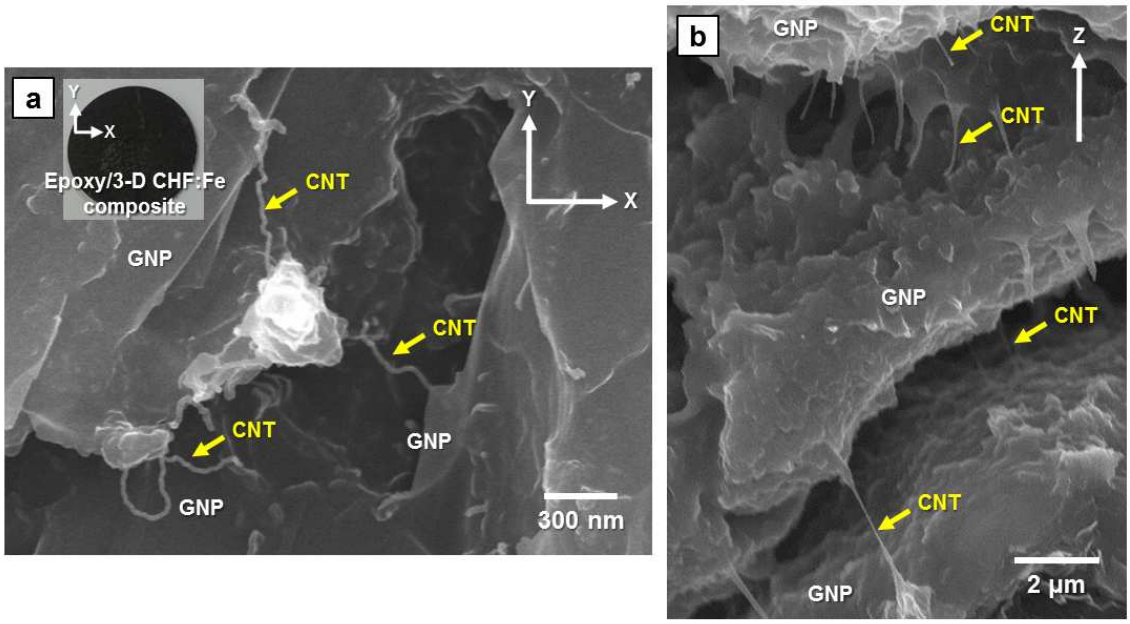

Fig. 6. (a) Experimental procedure for fabricating the 3-D CHFs from Fe-Co bimetallic nanoparticles. (b), (c) Surface morphologies of 3-D CHF:Fe-Co. (d), (e) TEM images of CNTs within a 3-D CHF:Fe-Co. (f) Comparison of thermal conductivities of epoxy composites with GNP, 3-D CHF:Fe, and 3-D CHF:Fe-Co fillers at 20 wt% total filler-loading.

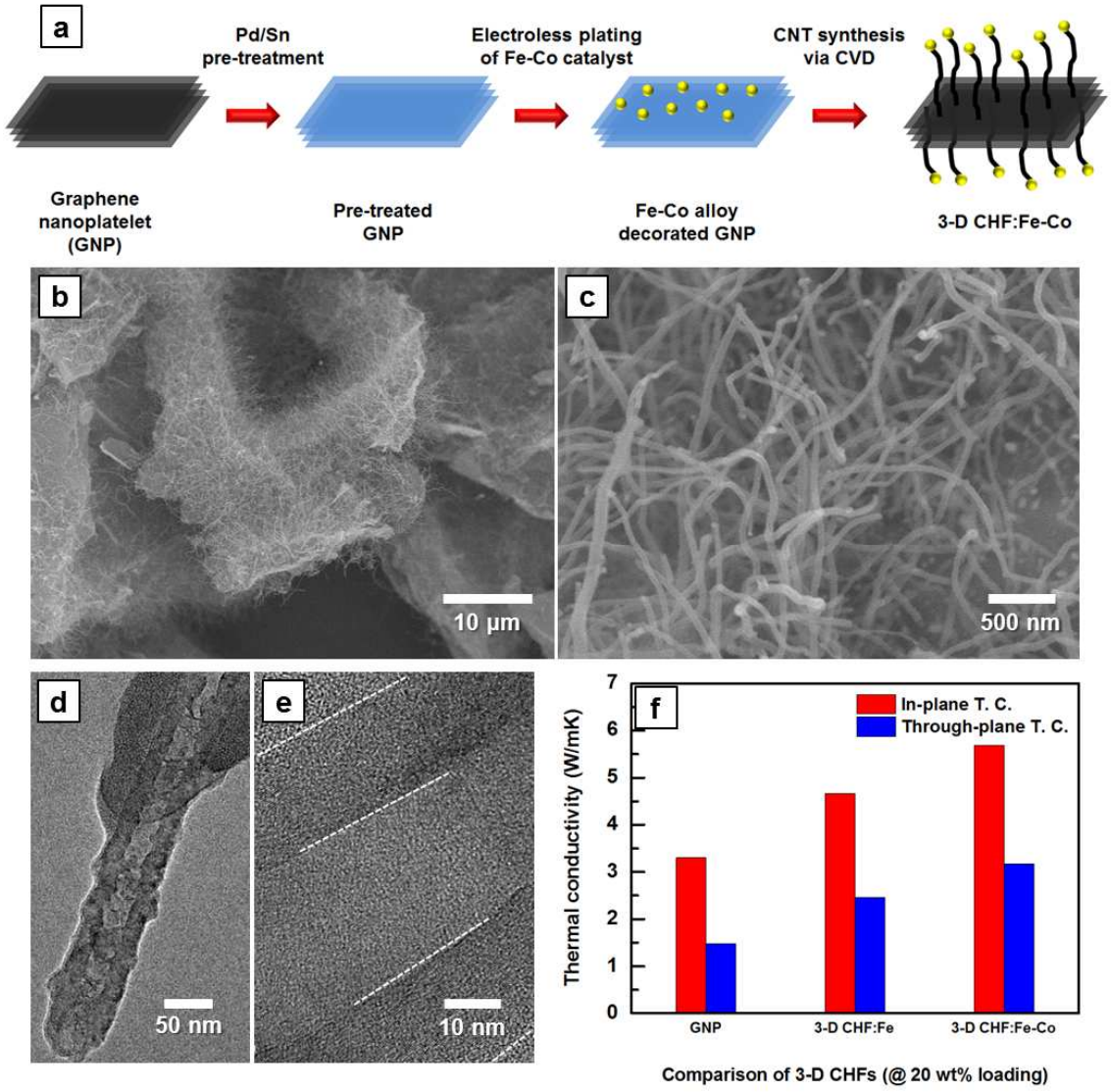

Fig. 7. Surface morphologies of calcined epoxy/3-D CHF:Fe-Co composites: (a) Plane view and (b) cross-sectional view. (c) Raman spectra of CNTs within a 3-D CHF:Fe-Co. (d) Comparison of thermal conductivities of epoxy composites with 3-D CHF:Fe-Co, 3-D CHF:Fe, and GNP fillers at 46.5 wt% total filler-loading.